UNIVERSIDAD DE ANTIOQUIA

FACULTAD DE CIENCIAS EXACTAS Y NATURALES

INSTITUTO DE FÍSICA

Baryon acoustic oscillations in the dark matter halos in the SDSS

Nataly Mateus Londoño

FACom, Grupo de física y astrofísica computacional

Instituto de física

Facultad de ciencias exactas y naturales

Advisor: Juan Carlos Muñoz Cuartas

UNIVERSIDAD DE ANTIOQUIA

FACULTAD DE CIENCIAS EXACTAS Y NATURALES

INSTITUTO DE FÍSICA

Baryon acoustic oscillations in the dark matter halos in the SDSS

AUTHOR:

_____

(Nataly Mateus Londoño)

ADVISOR:

_____

(Professor Juan Carlos Muñoz Cuartas)

Contents

Introduction

In the standard model of cosmology the universe was born in a big bang, an explosion that produced an expanding, isotropic and homogeneous Universe. From observations it has been found that this expansion is currently accelerating with time (Hamuy et al.,1996).

There are several components of the matter-energy content of the universe, dark and baryonic matter, radiation and dark energy. According to recent estimations, the last one accounts for around 70% of this content and is responsible for the accelerated expansion of the universe. The baryonic acoustic oscillations allows to study the nature of this expansion as it will be explained.

In the early universe the dark matter (DM) formed density fluctuations, causing baryonic matter to be unstable against gravitational perturbations. At this stage in the evolution of the universe the temperature was very high, allowing a coupling between baryonic matter and radiation through Thomson scattering. So the increase of baryonic matter in the DM density fluctuations not only caused an increase in density, but also radiation pressure against collapse. Therefore, an expanding wave centered in the fluctuation is caused because of the radiation pressure. This wave is the baryonic acoustic oscillation (BAO) (Hu and Sugiyama, 1996; Eisenstein and Hu, 1998).

Nevertheless, it is necessary to consider that the universe is expanding and this results in a temperature decrease. Therefore, when temperature is low enough the baryonic matter and

radiation decoupled, making BAO to stop expanding and leaving an imprint in the matter distribution. The distance that a BAO could have travelled by the time of decoupling is called sound horizon. This scale has been measured in the Cosmic Microwave Background as $146.8 \pm 1.8\text{Mpc}$, ([**?**]).

Since BAO do not change in size after decoupling they can be used as a standard ruler. They allow to measure the Hubble parameter and angular diameter distance as a function of z, and this way to measure the rate of expansion at different times during the evolution of the universe. Hence, BAO is key to constraint dark energy parameters.

A way to observe the imprint let by BAO is through the 2D point correlation function or the power spectrum that is its fourier pair, ([**?**], [**?**]). A peak due to the BAO appears in the correlation function (see figure 2.5) but there are several issues to take into consideration. There is a bias between baryonic and dark matter distribution ([**?**]) and hence in their correlation functions. This bias plays an important role when observational data is being studied. A method proposed in such cases is suggested in ([**?**]). Moreover, the non-linear clustering smear out the BAO imprint causing a broadening of the peak (Crocce and Scoccimarro, 2008). These, among other problems, have to be taken into account when BAO are studied.

Observational studies of baryonic acoustic oscillations have been done in several previous works such as [**?**], [**?**], [**?**], [**?**] . Measurements of baryonic acoustic oscillations on simulations have also been done in these works by [**?**], [**?**], [**?**], [**?**]. And theoretical studies of baryonic acoustic oscillation using non linear theory have been realized in [**?**], [**?**], [**?**], [**?**] .

In the present work, we plan to do a comparison between the power spectrum estimated from numerical cosmological simulations and the one obtained from observations of the Sloan Digital Sky Survey (SDSS). In both cases, observations and numerical cosmological simulations, the BAO peak will be studied, but what are the changes of the BAO's properties with changing the scale of the tracer halo population? is there any change in the position peak? is there any change in the width peak? or, is there a damping in the oscillations caused by BAO in the power spectrum? In general, the question we want to answer is: Is there any dependence in the width and amplitude of the BAO signal with the tracer halo population? Answering this questions will lead not only to profound understanding of the physics of BAO

but a better understanding of the accelerated expansion of the universe that still has so many questions to be answered.

1.1 Baryonic acoustic oscillations

Cosmological Background

Cosmology is the branch of physics that studies the Universe as a whole, therefore, it attempts to explain its origin, evolution and structure at big scales. Hence, a coarse grained approximation is mandatory due to the scales considered, this is, several approximations are necessary in the endeavour of such a task.

In this search, two major points are considered. The first one is the cosmological principle, it assumes that on sufficiently large scales the Universe is homogeneous and isotropic. In this context, homogeneity can be understood like invariance under translation and isotropy like invariance under rotation. Then, this principle establishes that for certain observers the Universe should appear isotropic and homogeneous, the fundamental observers. Since the Universe is expanding, the distance among fundamental observers changes with time but in an uniform way. Using these observers it is possible to synchronize clocks with a light pulse, the time measured by them is named cosmic time.

The overall isotropy and homogeneity have been found in observations of the cosmic microwave background radiation (CMB) and the sponge like structure of the distribution of galaxies. Until few years ago, all observations have agreed with this asseveration, however, recent evidence from Planck data have shown that anisotropies can appear at big scales [1].

The sponge like structure refers to the fact that, nowadays at cosmological scales, big structures such as halos, sheets and voids forming a filamentary distribution are observed. They are explained through the growth of initial seeds, small density perturbations at the

early Universe that evolve due to gravitational instabilities. These processes are occurring in an expanding Universe. This latter affirmation is predicted by the theory of general relativity in which modern cosmology is based, a second important point to consider. Here, Einstein field equations (EFE) serve as a set of fundamental equations to study the evolution of the Universe at big scales. Fortunately, isotropy and homogeneity led to a simple form of these ones and hence a relatively simple mathematical treatment in cosmology may be developed. From EFE, Friedmman equations are obtained which provide a theoretical framework to study the Universe expansion.

A standard model in cosmology that takes into consideration the aspects exposed previously is ΛCDM, where additionally to an expanding universe, there is a dark energy component that accelerates its expansion. This is precisely the framework that is going to be used in this work.

In this chapter, several basic concepts in ΛCDM standard model are going to be introduced to finally lead to bayronic acoustic oscillations (BAO). Several textbooks and articles were used as reference for this chapters such as [2], [3], [4].

2.1   Robertson Walker Metric

As was mentioned before, observations of the Universe at big scales show that it is homogeneous and isotropic, at least as a good approximation, i.e., inhomogeneities appear also at big scales in the CMB. Nevertheless, it is taken as a postulate for ΛCDM cosmology . Let's see this in more detail

- Cosmological principle: *The Universe is homogeneous and isotropic at big scales.*

  In this context, homogeneous refers to that the fact that independently of where the reference system is located we are going to observe the same global patterns, i.e., the structure of the observed Universe is the same no matter the reference system used. On the other hand, isotropy establishes that regardless of the direction chosen, the same structure is going to be observed. Then, we are dealing with translational and rotational symmetry.

  These characteristics are observed on mega parsec scales, i.e., big scales. However, this is only valid for the actual epoch, the scale changes with time due to the expansion of the Universe.

- Weyl postulate : *Establishes that the geodesics, world lines of galaxies, do not intersect except in a singular point in the past.*

  This one defines a set of observers that move along the geodesics. The interception point allows to synchronize watches among different observers, defining a cosmic time. Therefore, the distance between galaxies can be measured at the same cosmic time.

As already stated the Universe is expanding. It was due to a research on nearby galaxies performed by Edwin Hubble that a redshift was found in most of the galaxies, i.e., they are moving away from us. Considering this movement, one could conclude we are in the center of the expansion. But this conclusion is wrong since the expansion Hubble law is valid independently where the coordinate system is defined.

A metric that satisfies homogeneity and isotropy and additionally contains a term that accounts for the Universe's expansion is the Robertson Walker metric. It is defined in general terms as $ds^2 = g_{\mu\nu}dx^\mu dx^\nu$, where $g_{\mu\nu}$ is the metric tensor and uses coordinates $x^\alpha = \{ct, x, y, z\}$. The metric tensor takes the next form $g_{\mu\nu} = diag\{1, -\frac{a^2}{1-k^2} - a^2 r^2, -a^2 r^2 \sin^2\theta\}$, and the metric is

$$ds^2 = c^2 dt^2 - a(t)^2 \left[\frac{d^2 r}{1 - Kr^2} + r^2(d^2\theta + \sin^2\theta d^2\phi) \right] \tag{2.1}$$

The term $a(t)$ is the scale factor, it describes how the relative distance between two fundamental observers changes with time. The term K is the curvature constant for the actual time and defines the Universe geometry. When $K = 0$ an euclidean metric is recovered leading to a flat universe expanding indefinitely. If $K = 1$ the Universe would be described by a spherical geometry and it would collapse because of its energy matter density content. And finally, $K = -1$ corresponds to a hyperbolic geometry where the Universe would be in accelerated expansion. In the figure 2.1 we show the behavior of different cosmologies depending on the K value and density content.

One important aspect to consider is that the geometry depends on the total energy-matter density content, Ω_o. This can be concluded from the definition of the curvature constant $K = H_o^2(\Omega_o - 1)/c^2$.
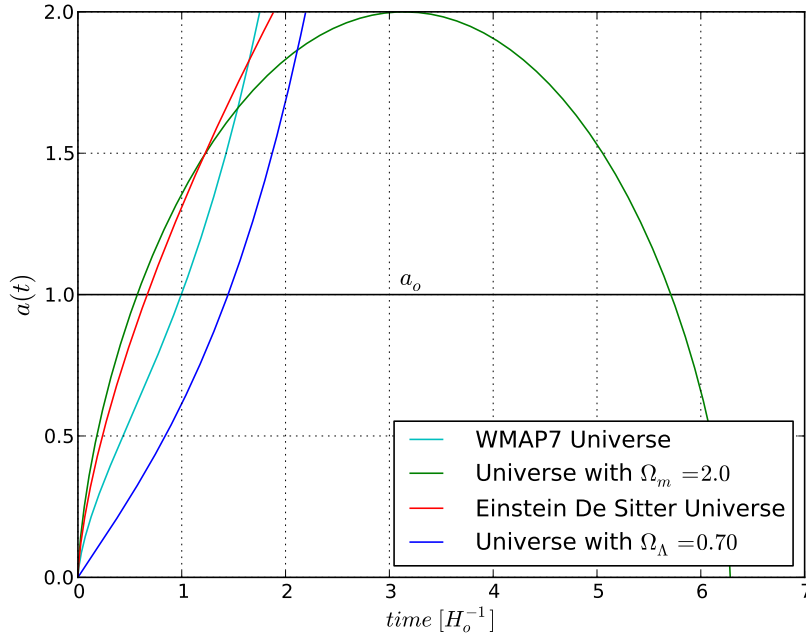
Figure 2.1: Scale factor as a time function. The Universe expansion for different density contributions. A closed Universe is obtained when $\Omega_m = \Omega_o > 1$. Also, the PLANCK parameters show an accelerated expansion.

2.2 Hilbert-Einstein field equation

At big scales, the most important fundamental interaction of nature is the gravitational one. Hence, the theory of general relativity (TGR) is an essential tool in the study of the cosmos.

At smaller scales, the Newtonian gravitational theory might be used, where the Poisson equation offers a relation between the second derivative of the gravitational potential Φ and the source of the field ρ

$$\nabla^2 \Phi = 4\pi G \rho$$

this equation is obtained from TGR for low velocities and a weak gravitational field ($\Phi/c^2 << 1$). A key equation of TGR is the Hilbert-Einstein field equation, a 6 independent component tensorial equation

$$R_{\mu\nu} - \frac{1}{2}g_{\mu\nu}R - g_{\mu\nu}\Lambda = \frac{8\pi G}{c^4}T_{\mu\nu} \tag{2.2}$$

in equation 2.2 the first term of the left side is Ricci's tensor (second derivatives of the metric tensor). The second one contains the scalar of curvature R that defines space-time

geometry. In the third term, Λ is the cosmological constant that could be associated with the vacuum density term and is responsible for the accelerated expansion of the Universe.

In the right side of the equation, the tensor energy-momentum $T_{\mu\nu}$ is present. It includes, as its name suggest, all the contributions to energy and momentum.

Hence, the left side of the equation has associated geometry terms, while the right one, the ones associated with the matter and energy distribution. Then, it could be interpreted as if geometry is determined by the matter-energy content of the Universe, though, strictly speaking, the energy-momentum tensor depends in the metric tensor too.

There is an interesting case of this tensor when we are dealing with a perfect fluid, i.e., without viscosity. It shows that not only density causes curvature of space-time but also pressure. The Universe can be modeled with this particular shape of the energy-momentum tensor. It can be expressed as

$$T_\sigma^\mu = diag\{c^2\rho, -P, -P, -P\}$$

where ρ is the density and P is the fluid pressure.

There are several solutions to the Einstein field equation but not many in an analytical form. An analytical solution is Schwarzchild's solution that represents the metric of a static spherical mass. Other possible solution is the Kerr metric that corresponds to a rotating uncharged mass. The Robertson Walker metric satisfies these equations too.

2.3   Friedmann equations

From HE field equations and the RW metric is posible to propose cosmological models that give account for the observed dynamics in the Universe. In this direction, the components of the field equation can be taken, $\beta = \nu = 0$, time-time component, and $ii = 1, 2, 3$ (space-time components), from where

$$\frac{\ddot{a}}{a} = -\frac{4\pi G}{3}\left(\rho + 3\frac{P}{c^2}\right) + \frac{\Lambda c^2}{3} \tag{2.3}$$

$$\frac{\ddot{a}}{a} + 2\frac{\dot{a}^2}{a^2} + 2\frac{c^2 K}{a^2} = 4\pi G\left(\rho - \frac{P}{c^2}\right) + \Lambda c^2$$

here, it has been used the energy momentum tensor for an ideal fluid. The former expressions are the Friedmann equations and give account of Universe expansion dynamics. The

terms involved are the scale factor $a(t)$ and it is equal to one for the actual epoch, $a(t_o) = 1$, also ρ is the radiation and matter density, P is the total pressure.

The equation 2.4 has the form of force equation and it can be parcially deduced from newtonian mechanic (without the presion and cosmological constant terms). A most convenient and used form is obtained after algebraically manipulating them

$$H(t) = \frac{\dot{a}^2}{a^2} = \frac{8\pi G}{3}\left(\rho + \frac{\Lambda c^2}{8\pi G}\right) - \frac{Kc^2}{a^2} \tag{2.4}$$

this one can be interpretated as an energy equation, where the first term in the right hand side is the potential energy. This equation also allows to define the Hubble parameter and for the actual epoch this coincides with the Hubble constant $H(t_o) = H_o = 100h$ Km s^{-1} Mpc^{-1}.

Aditionally 2.5 can be expressed in terms of the critical density, i.e.m the matter and energy amount neccesaries for the Universe to be flat. Therefore, if the Universe has a bigger density it would collapse about itself. Conversely, the Universe would continue to expanding indefinitly. This quantity is defined as $\rho_{crit}(t) = 3H(t)^2/8\pi G$.

Dividing 2.5 by the Hubble constant H_o and defining the density parameter $\Omega_{i,o} = \rho_{i,o}/\rho_{crit}(t_o)$ with $i = m, r, \Lambda$ is obtained

$$\frac{H^2(z)}{H_o^2} = \Omega_{m,o}\left(1+z\right)^3 + \Omega_{r,o}\left(1+z\right)^4 + \Omega_{\Lambda,o} + \left(1 - \Omega_o\right)\left(1+z\right) \tag{2.5}$$

where $\Omega_o = \Omega_{m,o} + \Omega_{r,o} + \Omega_{\Lambda,o}$. It has been introduced the relation between redshift and scale factor $1 + z = 1/a$. The different contributions to the density to the Hubble parameters are observed, i.e., the matter, radiation and vacuum density. Every component is a function of the Universe expansion, although the vacuum energy does not depend on the redshift, this is, is constant through time.

Initially the Universe was dominated by the radiation, during this epoch matter and radiation were coupled, i.e., the De Broglie electrons wavelenght were comparable to the radiation one. Because of this, the photons free mean path is negligible causing the Universe to be opaque.

During this coupling, the radiation temperature is equal to the matter one and its behaviour is explained as a black body.

As can be seen in the plot 2.2, from $z = 3230$ matter becomes the major contribution to the Universe density. When $z = 1100$ the temperature drop is big enough for the recombination

rate gets higher than the ionization one. Recombination refers to the formation of neutral atoms, that was the ultimate cause to decoupling.

The last radiation dispertion due to matter still can be observed, and it is called cosmic radiation background (CMB). Because of the Universe expansion, its temperature has been dropping, and it is nowadays around $T = 2.7K$.
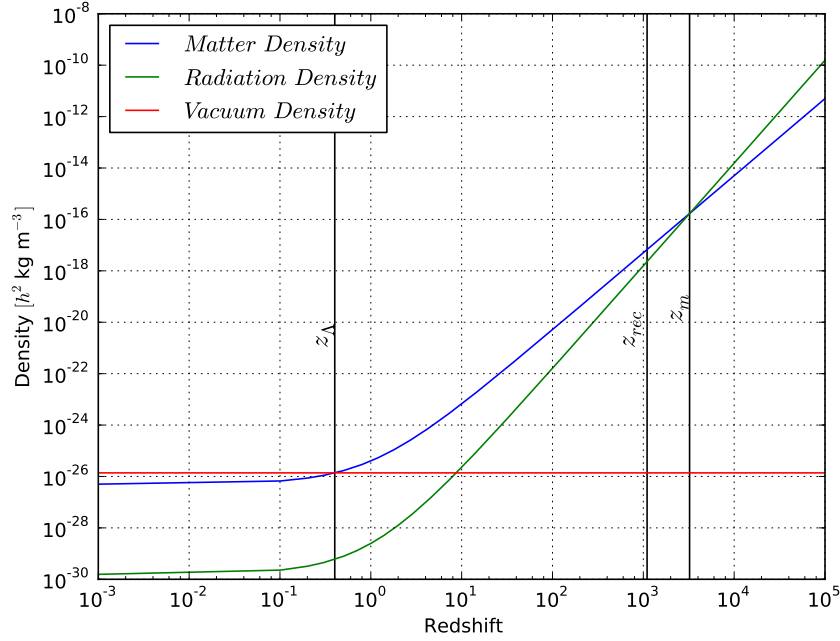

Figure 2.2: Dependence in redshift for Ω_Λ, Ω_m and Ω_r. The decoupling between matter and radiation is obtained when z_{rec}.

Nowadays, the dominant density component is vacuum, though it is a constant since it does not depend on the scale factor $\rho_\Lambda = -c^4\Lambda/8\pi G$, in contrast with matter, which depends on it as a^{-3} and radiation as a^{-4}, causing both components diminish in time.

The cosmological constant is associated to vacuum energy that causes an opposed behaviour in the Universe dynamics compared to mass density, i.e., it gives account for the accelerated universe expansion.

There are several solutions to 2.5, for instance in the Einstein de Sitter Universe, there are no radiation or vacuum contributions to the density and the total density is $\Omega_o = 1.0$. In this particular case, the solution is

$$t = \frac{2}{3H_o}(1 + z)^{-3/2}$$

Therefore, depending on the chosen density values, the equation 2.5 has different solutions

Parameter	Symbol	Best fit
Hubble constant ($km/Mpc - s$)	H_0	68.65± 0.93
Baryon density	$\Omega_b h^2$	0.02248±0.00044
Cold dark matter density	$\Omega_c h^2$	0.1165±0.0024
Dark energy density	Ω_Λ	0.705±0.0011
Scalar spectral index	n_s	0.967± 0.01
Sigma 8	σ_8	0.830

Table 2.1:   Fit cosmological parameters from WMAP+BAO nine-year results.

and one can expect several Universe models, i.e., depending on the parameters chosen, the Universe evolution changes. In the case of WMAP9, the parameters used are shown in table[1] 2.1.

Other possible Universe models are for example, one obtained when matter density parameter is the only contribution to total universe density but it is bigger than 1. In such case the Universe obtained is closed. Other one, it is one obtained when the Universe is dominated for the vacuum contribution. In this case, the Universe is always open. When all the contributions are present, the Universe can be open or closed depending on the total density paremeter.

2.4   Equation of state

As mentioned before, scale factor determines the Universe expansion, hence it is mandatory to find relations that relates the different universe density components with it.

Assuming matter is an isolated system, the first law of thermodynamics is expressed as $dU = -pdV$, where relativistic terms are included in the internal energy term. Using the equipartition theorem and derivativing internal energy with respect to scale factor is obtained

$$T \propto a^{-2}$$

but from the equation state $P = NkT$ and taking into account that $N = N_o a^{-3}$ it is known that $P \propto a^{-5}$. Pressure due to matter diminishes strongly with Universe expansion, while density and temperature change smoother. The latter is another cause for vacuum to dominate the Universe expansion.

---

[1]Table taken from `https://lambda.gsfc.nasa.gov/product/map/dr5/params/lcdm_wmap9.cfm`

Radiation energy density is

$$\xi = \sum_{\nu} N(\nu) h\nu$$

where $N(\nu)$ is photon density and satifies the relation $N \propto (1+z)^3$, so that $\xi \propto \sum_{\nu} C_{\nu} a^{-4}$. Comparing with Stefan Boltzmann law is concluded that $T \propto a^{-1}$. Radiation pressure dependence on scale factor is found using $P = \frac{1}{3}\epsilon_{total}$ with which is obtained $P \propto a^{-4}$.

Otherwise, vacuum satisfies $\epsilon_{total} = \rho c^2$ where ρ is an effective density. Replacing this result in the first law of thermodynamics and derivativing with respect to scale factor

$$P = -\rho c^2 = -\frac{\Lambda c^4}{8\pi G}$$

the vacuum density constancy has to be used in its deduction.

2.5 Perturbation evolution in the newtonian regimen

As already stated, there is no radiation comming toward us from a previous epoch to decoupling. Although, due to the last scattering between radiation and matter, highly homogeneous and isotropic distribution of matter is observed, i.e., patterns obtained from background cosmic radiation[2] (Figure 2.3).

In the CMB radiation, small temperature perturbations are observed indicating precisely the presence of small matter perturbations at this epoch. These are the initial seeds from where structures observed nowadays formed.

At the present time the wavelength associated to this cosmic radiation is in the microwave range.

In this structure growth, density fluctuations are increasing but it is not until they got a size of $\delta \sim 1$ that their movement was not exclusive due to the cosmic expansion. The fluctuations have grown enough to start talking about galaxy formation when their density gets around 1×10^6 compared with the background density, this happens for a epoch around $z \sim 100$.

But, it is still important to study the initial stages of the fluctuations. Because of this, a linear regime treatment for fluctuations when $\delta \ll 1$ are key in such a study.

---

[2] Image WMAP taken from `http://lambda.gsfc.nasa.gov/product/map/current/m_images.cfm`
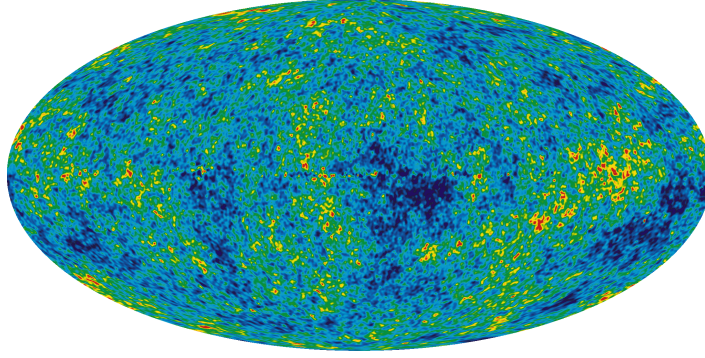
Figure 2.3: Cosmic background radiation image obtained by WMAP using 5 different maps.

2.5.1   Newtonian description

Inhomogeneities have to be formed at initial stages, these initial density fluctuations have a characteristic length much smaller than the Hubble radius. This implies that the size of the fluctuations is very small compared with scales where the Universe curvature is significant, making this Newtonian approximation be valid. Because of this, casualty is taken as granted.

Basic equations of gas dynamics for a fluid in motion of density ρ subject to a gravitational field that suffers changes in pressure satifies

$$
\begin{aligned}
\frac{d\rho}{dt} &= -\rho \nabla_r \cdot \mathbf{u} \\
\frac{d\mathbf{u}}{dt} &= -\frac{\nabla_r P}{\rho} - \nabla_r \phi \\
\nabla_r^2 \phi &= 4\pi G \rho
\end{aligned}
\tag{2.6}
$$

As density fluctuations are more of our interest, since inhomogeneties respect to background are the ones that trigger potential wells, it is useful to expresss density as $\rho = \overline{\rho} + \delta\overline{\rho}$, where $\overline{\rho}$ is the background density. Here, it is necessary to clear another point. Particle velocities have two different contributions, the first one is caused because of the Universe expansion and the other one is the proper velocity of the particle,recessional and peculiar velocities respectively. From the latter mentioned, the coordinate system can be changed from 2.6 an Euler description to a Lagrangian one, i.e., moving with the Universe expansion. Let's see this in more detail, velocity in an Eulearian description is $\mathbf{u} = a\dot{\mathbf{x}} + \mathbf{x}\dot{a} = \mathbf{v} + \mathbf{x}\dot{a}$, where $\mathbf{v}$ is the peculiar velocity and $\mathbf{x}\dot{a}$ is the Universe expansion velocity. Then, making a change to comovil coordinates, coordinates that move with the Universe expansion and changing density to density contrast, the next equations are found

$$
\begin{aligned}
\frac{\partial \delta}{\partial t} &= -\frac{1}{a}\nabla \cdot [(1+\delta)\mathbf{v}] \\
\frac{\partial \mathbf{v}}{\partial t} + \frac{\dot{a}}{a}\mathbf{v} + \frac{1}{a}(\mathbf{v}\cdot\nabla)\mathbf{v} &= -\frac{\nabla\Phi}{a} - \frac{\nabla P}{a\overline{\rho}(1+\delta)} \\
\nabla^2\Phi &= 4\pi G\overline{\rho}a^2\delta
\end{aligned}
\tag{2.7}
$$

the first one corresponds to the continuity equation, the second one is Euler's equation and the last one is poissonian gravitational field equation. Velocity components appear due to gravitational interactions and changes in pressure, here Φ is an effective potential.

Aditionally, equation of state relating the thermodynamic quantities P, ρ and s (entropy) for this cosmological fluid is

$$
P(\rho, s) = \left[\frac{h^2}{2\pi(\mu m_p)^{5/3}}e^{-5/3}\right]\rho^{5/3}\exp\left(\frac{2}{3}\frac{\mu m_p s}{k_B}\right)
\tag{2.8}
$$

Manipulating algebraically the continuity equation, Poisson equation and state equation, a wave equation for density fluctuations can be obtained

$$
\frac{\partial^2\delta}{\partial t^2} + 2\frac{\dot{a}}{a}\frac{\partial\delta}{\partial t} = 4\pi G\overline{\rho}\delta + \frac{C_s^2}{a^2}\nabla^2\delta + \frac{2}{3}\frac{\overline{T}}{a^2}\nabla^2 s
\tag{2.9}
$$

where $\overline{T}$ is the background temperature and C_s is the speed of sound. The Universe expansion is seen in the second term in the left side. Since for an expanding Universe the term $\dot{a}a$ is positive, Hubble parameter, its effect is opposed to the perturbation growth. This result was expected due to expansion is against collapse leaving to a decrease in growth.

In the right side causes for perturbation evolution are shown, these can make them grow or disipate. Entropy can be considered as heat interchange between perturbation and surroundings, causing the expansion or growth of the perturbation. As expected, gravitational field is a source for perturbation growth.

A solution to the perturbation equation in terms of Fourier series is proposed

$$
\begin{aligned}
\delta(x, t) &= \sum_k \delta_k(t)e^{ik\cdot x} \\
s(x, t) &= \sum_k s(t)e^{ik\cdot x}
\end{aligned}
$$

$\mathbf{k}$ is the wave number and δ_k is a density mode that can be calculated using the discrete Fourier transform of the density field. Hence, every mode depends on all known values of the density perturbations.

An important aspect in the last expression is the indepencency of the functions $e^{ik\cdot x}$ allowing equation 2.9 be expressed as

$$\frac{d^2\delta_k(t)}{dt^2} + 2\frac{\dot{a}}{a}\frac{d\delta_k(t)}{dt} = \left[4\pi G\overline{\rho} - \frac{C_s^2 k^2}{a^2}\right]\delta_k(t) - \frac{2}{3}\frac{\overline{T}}{a^2}k^2 s_k(t) \qquad (2.10)$$

the solution of the equation provides expansion coefficients for the Fourier series, from where, the behaviour of density fluctuations, their growth or disipation, is obtained.

2.5.2   Jeans Inestability

Before solving the mode equation 2.10, it is important to develop some intuition about the physical phenomena. This can be achived making some simplifications. For example, taking an isentropic static Universe ($\dot{a} = 0$) the expression becomes

$$\frac{d^2\delta_k(t)}{dt^2} + \omega^2\delta_k(t) = 0$$

with $\omega^2 = C_s^2 k^2/a^2 - 4\pi G\overline{\rho}$. Clearly the solution of modes equation depends on ω's sign, if $C_s^2 k^2/a^2 > 4\pi G\overline{\rho}$, ω is positive and the solution obtained is oscillatory. In other words, this solution is a sound wave not gravitationally inestable, therefore, it is not of our interest. By the other side, if $4\pi G\overline{\rho} > C_s^2 k^2/a^2$ the solution takes the form $\delta_k(t) \propto e^{\Gamma_k t}$, with $\Gamma_k = i\omega_k$ named growth rate. In this case, the perturbation disipates or collapses depending on the square frequency sign chose.

Physically, it is expected fluctuations tend to collapse because of gravity though preassure gradient caused by atomic interactions goes against it. The ones of interest are those that collapse. For this, a minimum length that a perturbation must have to obtain an inestable fluctuation, i.e., a collapsing perturbation, is defined. Hence, from the frequency Jeans' length is obtained $\lambda_J = 2\pi a/k_j$ and satisfies $\lambda_J = 2\pi/k_j = C_s(\pi/G\rho)^{1/2}$. The growth rate can be rewritten in terms of λ_J, allowing to make the next comparison, if $\lambda_{pert} >> \lambda_J$ is satisfied the perturbation collapses, here λ_{pert} is the length of the perturbation.

As was shown previously, Jeans' length depends on the speed of sound that is defined as

$$C_s^2 = \left(\frac{\partial P}{\partial \rho}\right)_s$$

and using also the equation of state 2.8 a relation is found. It was also used the fact that radiation and matter temperature are equal for $z \leq z_{eqv}$ due to coupling. But after decoupling every component evolves independently. Jean's length and mass, the last one defined as $M_J = \pi\overline{\rho}_{m,o}\lambda_J^3$, are given by

$$\lambda_J \approx 0.01(\Omega_{b,o}h^2)^{-1/2}Mpc \tag{2.11}$$

$$M_J \approx 1.5 \times 10^5(\Omega_{b,o}h^2)^{-1/2}M_\odot \tag{2.12}$$

Before decoupling, speed of sound was affected not only by matter but for radiation, even the latter one was more important since radiation density dominates in this epoch (figure 2.2). The valid state equation for radiation in this epoch is $P = c^2\rho_r/3$ and it can be shown that the change in magnitude order evaluated before and after decoupling of Jean's length and mass is 2.6×10^{-5} and 1.8×10^{-14} respectively. From previous asseveration a possible conclusion is decoupling increases gravitational collapse since minimum characteristic length required for collapsing becomes smaller.

Until now dark matter has not been mentioned, a component that contrary to baryonic matter does not interact with radiation. But it is around 23% of the overall Universe content, making it responsible for the large scale mass distribution observed. Dark matter particles interact among them and with baryonic matter through gravitational interaction. This leads to dark matter potential wells where baryonic matter can also fall. It occurs around $z \sim 3500$. But, dark matter initial seeds for potential wells are formed before decoupling, since they do not interact with radiation, they can gather forming them. While this happens, baryonic matter and radiation interacts gravitationally with dark matter, leading to no formation of baryonic seeds precisely because of the mentioned coupling. Later a more detailed explanation will be provided.

The last arguments exposed allow to express perturbations as $\delta = \delta_o D(z)$, where δ_o is an initial seed from where a dark matter potential well formed and $D(z)$ is a growing function of an initial seed. Then, rewritting equation 2.10

$$\frac{d^2D(z)}{dz^2} + \left[\frac{H'(z)}{H(z)} - \frac{1}{1+z}\right]\frac{dD}{dz} = \frac{1}{H^2(z)}\left[\frac{4\pi G\overline{\rho}(z)}{(1+z)^2}\right]D(z)$$

in the expresion isotropy was assumed and the velocity term was neglected since the perturbations of our interest satify $\lambda_J \ll \lambda$. Using the last equation, different solutions changing density parameters are obtained. For example, an Einstein de Sitter Universe $\delta_k(z) = \delta_o(1+z)^{-1}$, an Universe dominated by radiation $\delta_k(z) = \delta_o(1+z)^{-1.22}$ and an Universe dominated by vacuum $\delta_k(z) = \delta_o(1+z)^{-0.58}$. Obviously, for different contributions to every component of density can be found, in figure 2.4 is shown perturbations evolution for a model with matter and vacuum contributions. As expected, for bigger matter density
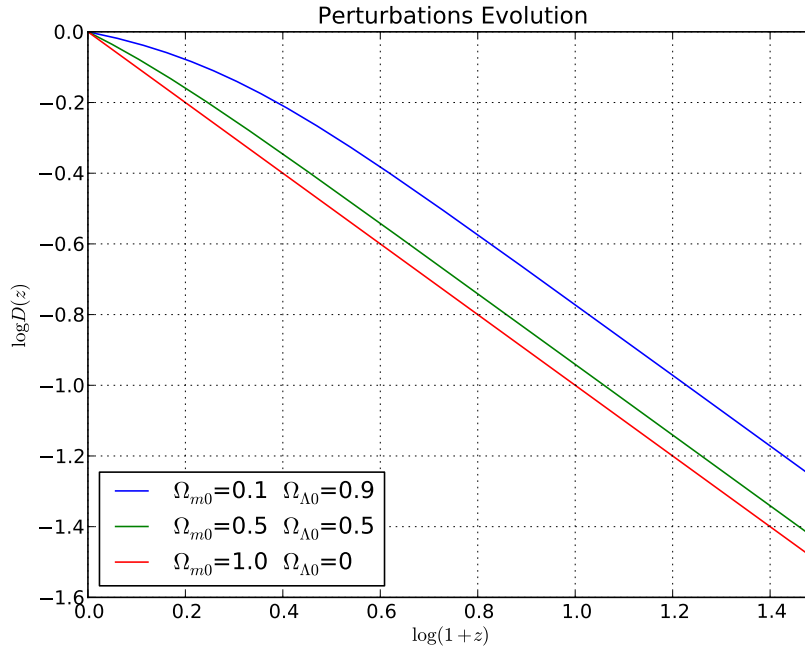
Figure 2.4: Perturbation evolution for a model Mass-vacuum, the behaviour for different contributions of each component.

perturbations grow faster while for universes with bigger vacuum contribution, perturbations grow slower cause accelerated expansion. In the latter, a bigger initial mass is required to start collapsing. In the figure, largest redshift is $z = 0$ but solution is only valid while $\delta \ll 1$.

2.6   Higher order perturbation theory

As mentioned, perturbations start growing after decoupling. This growth leads precisely to an increase in their density contrasts. When they have increased enough, around $\delta \sim 1$, Newtonian description stops being valid. A first approach to study such perturbations is spherical collapse. Even for those δ values, perturbations are not considered an object. In such cases, gravitational interaction determines dynamics more than Universe expansion. This ocurrs when density gets around $\sim 100\overline{\rho}$.

Now, let's see in more detail spherical collapse. In this scenario a perturbation has spherical symmetry and pressure exerted among particles is neglectable. But the latter supposition would imply that collapsing cause perturbations to end up as a singularity, since there is no force against collapse. If tidal forces are included it would not be the case but it is taken as a first approximation.

Time calculated for a perturbation to collapse is

$$1 + z_c = \frac{1 + z_{max}}{2^{2/3}}$$

where z_{max} is redshift when perturbation dynamics is no longer affected by Universe expansion. Collapsing time for a perturbation is smaller than time necessary to become a gravitationally linked object. Aditionally redshift estimative for a perturbation satisfies virial theorem is

$$(1 + z_{vir}) \leq 0.47 \left(\frac{v}{100 km s^{-1}} \right)^2 \left(\frac{M}{10^{12} M_{\odot}} \right)^{-2/3} (\Omega_o h^2)^{-1/3}$$

it can be noticed from this expresssion that more masive objects and with a bigger dispersion velocity have a bigger viralization time.

2.6.1 Zeldovich approximation

The last model for a non lineal perturbartion treatment has several failures. A next step in this direction is Zeldovich approximation that provides a more realistic description, since it considers that fluctuations' shape is an ellipsoid. Though pressureless and without viscosity fluid supposition are still taken. Coomovil coordinates satisfies

$$\mathbf{x} = a(t)\mathbf{r} + b(t)\mathbf{p(r)}$$

where $\mathbf{r}$ are Eulerian coordinates and $b(t)\mathbf{p(r)}$ is the displacement respect to the initial position. The last term is related with the gravitational potential generated by initial perturbations. It can be shown that initial perturbations are given by

$$\rho = \frac{\overline{\rho}}{[1 - \alpha b(t)][a(t) - \beta b(t)][a(t) - \gamma b(t)]} a^3(t)$$

where α, β and γ account for the expansion or contraction along the three main axis of the ellipsoid. When $\alpha \geq \beta \geq \gamma$ and $b(t)$ are sufficiently big enough a singularity appears. If α also gets its highest value causes that fluctuations get a pancake shape due to a faster contraction in x axis. Despite of the simplicity, it is a model accurate with numerical results. Hence, it is used in observational cosmology and initial condition generation in N body simulations.

2.7 Statistical properties of cosmological perturbations

Nevertheless, to study the evolution of the Universe since decoupling requiere to know or assume a density field, to know density in every point and its evolution with time. But using

the concept of density contrast $\delta = (\rho - \bar{\rho})/\bar{\rho}$, leads to a density perturbation field, which is a clearer way to analyse the evolution of the density field.

In linear regime, there are a huge amount of perturbations described by different fourier modes. Since they evolve independently their amplitudes change with time and can be modelled using a transfer function $T(k)$ and a linear growth rate $D(t)$. To characterize such amount of density field values, statistical properties must be defined. This is, not considering individual positions or properties but instead moments defined from some distribution function. This idea is supported by the fact that there is no access to the primordial perturbations that originated the large scale structure observed nowadays. Hence, our Universe could be considered as a realization of a random process where a statistical treatment results as a natural way to study it.

Consider that the Universe can be divided into small cells, each of them with position x_i. These can be statistically characterized with a joint probability distribution and its moments that, in principle infinite, would describe the cosmic density perturbation field. Following this approach, the probability of having a mode between δ_k and $\delta_k + d\delta_k$ is,

$$\mathcal{P}(\delta_{\boldsymbol{\kappa}}) r_{\boldsymbol{\kappa}} dr_{\boldsymbol{\kappa}} d\phi_{\boldsymbol{\kappa}} = \exp\left[-\frac{r_{\boldsymbol{\kappa}}^2}{2V_u^{-1}P(\kappa)}\right] \frac{r_{\boldsymbol{\kappa}}}{V_u^{-1}P(\kappa)} \frac{dr_{\boldsymbol{\kappa}}}{2\pi} \frac{d\phi_{\boldsymbol{\kappa}}}{2\pi} \qquad (2.13)$$

where $r_{\boldsymbol{\kappa}}$ corresponds to perturbations amplitude, $\phi_{\boldsymbol{\kappa}}$ is the phase and varies between $[0, 2\pi)$. The joint probability distribution function is useful because it allows the independence of the terms $\delta_{\boldsymbol{\kappa}}$, or in other words it is the product of every mode

$$\mathcal{P}_{\boldsymbol{\kappa}}(\delta_{\boldsymbol{\kappa}1}, ..., \delta_{\boldsymbol{\kappa}N}) = \prod_{\boldsymbol{\kappa}} \mathcal{P}_{\boldsymbol{\kappa}}(\delta_{\boldsymbol{\kappa}})$$

This expression is not satisfied when the inverse fourier transform is done, since the probability density is not separable in the initial coordinate space. The term $P(\kappa)$ (assuming isotropy in $\boldsymbol{\kappa}$) is the power spectrum defined in the fourier space and it is related to the 2 point correlation function in the real space

$$P(k) = \frac{4\pi}{V_u} \int_0^\infty \xi(r) \frac{sin(kr)}{kr} r^2 dr = \langle |\delta(\boldsymbol{\kappa})|^2 \rangle \qquad (2.14)$$

as it can be seen in the expression, the isotropy of the universe is taken into account since during the power spectrum calculation, an average is done over all possible orientations of the vector $\boldsymbol{\kappa}$

Here, $\xi(r)$ describes the distribution of points, telling for example, how clumpy certain region is or in general the clustering properties of the system. Being more specific, this

function describes the excess probability of finding a particle at a distance r from a particle selected at random over the expected in an uniform, random distribution. The two point correlation is defined as

$$\xi(r) = \langle \delta(\mathbf{x})\delta(\mathbf{x} + \mathbf{r}) \rangle$$

therefore, the density field leads to a direct way to find the power spectrum through a fourier transform. ξ only depends on the amplitude of r because of the assumption of homogeneity and isotropy, i.e., depends on relative distances.

No clustering would imply that $\xi(r)$ is zero. A natural way to see this is through a conditional probability, given that there is a particle in a volume element dV_1 the probability there is other one in a volume element dV_2 at a distance r

$$dP(2|1) = n[1 + \xi(x_{12})]dV_2$$

if $\xi(x_{12}) > 0$ the probability of finding such pair of particles increases, i.e., there is clustering of structures. But if $\xi(x_{12}) < 0$ such probability diminishes leading to an anticorrelation. In the case where $\xi(x_{12}) = 0$ there would be no clustering, the distribution of particles would be the one of a random catalogue.

Also, the function $\xi(r)$ can be expressed as a power law of the form

$$\xi(r) = \left(\frac{r}{r_0}\right)^{-\Gamma}$$

being valid in the range $100h^{-1}$ kpc to $10h^{-1}$ Mpc. The preferred scale $r_0 = 5h^{-1}$ Mpc is the one where the galaxy density is greater than twice of the background. The exponent value is $\Gamma = 1.8$. This fit overestimates the correlation function for distances bigger than $20h^{-1}$ Mpc.

So far, it has been shown two statistical measures, a fourier pair, in real space the correlation function and in fourier space the power spectrum. But other moments can be specified as previously mentioned, in general an l point correlation function can be defined through the next expression $\xi^l(\vec{x}_1, \vec{x}_2, \ldots \vec{x}_l) \equiv \langle \delta_1 \delta_2 \ldots \delta_l) \rangle$ where the connected terms are the ones that contributed to the calculation. For example, the first moment of the distribution is $\langle \delta(x) \rangle = 0$ because of the definition of density perturbation field.

An important remark is that if initial density pertubations follow a gaussian distribution all moments higher than two (2 point correlation function) are zero, i.e., the density perturbation field is completely described by the two first moments of the distribution.
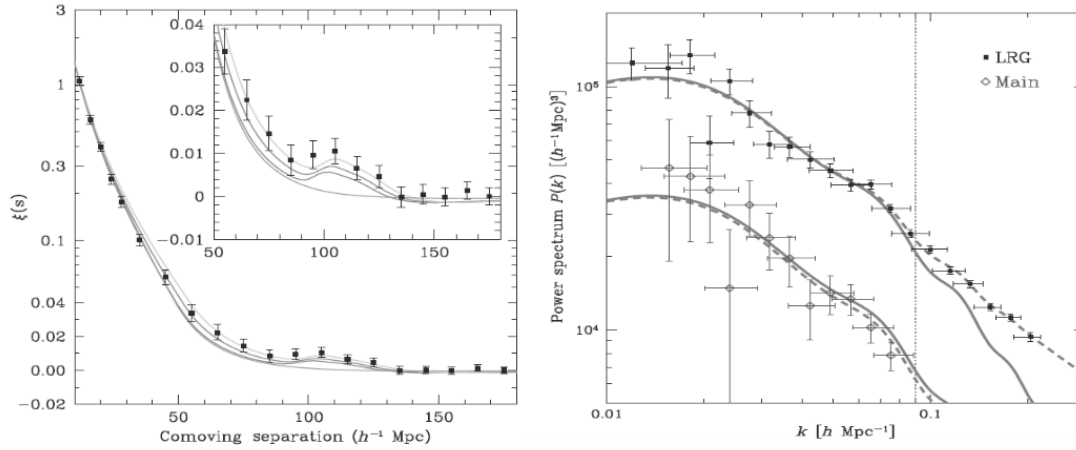
Figure 2.5: BAO peak in the correlation function in the left and the oscillations of BAO in the power spectrum in the right, ([**?**]). The lower curve is the main SDSS sample and the upper one is the LGR sample.

It is usually considered for the initial density field, that density contrasts follow a normal distribution centered in $\langle \delta \rangle = 0$. This idea is supported by inflationary scenarios where a random gaussian perturbation field arises naturally from quantum fluctuations during inflation, i.e., statistical behaviour lies on quantum fluctuations. Since there are a large number of modes, the central limit theory would support this idea if the mode phases are independent. One of the advantages of this model is that the perturbation field remains gaussian during linear evolution.

Additionally it has been found that the initial power spectrum expected from inflation theories has the form $P(\kappa) = k^n$. If $n = 1$ the power spectrum is called Harrison-Zeldovich which is commonly used.

With the initial power spectrum it can be done an inverse fourier transform and this way creating the initial density field.

Furthermore, using inflationary models the shape of the linear power spectrum is well determined but there are not amplitude predictions, i.e., there is not a defined normalization of the power spectrum. One commonly way to do such thing is through the variance of the galaxy distribution when sampled with randomly placed spheres at radius R. The relation between the variance of the density field and the power spectrum is

$$\sigma^2(R) = \frac{1}{2\pi^2} \int P(k)\hat{\omega}_R(k)^2 k^2 dk$$

where $\hat{\omega}_R(k)$ is the Fourier transform of the spherical top hot model.

$$\hat{\omega}_R(k) = \frac{3}{(kR)^2}[\sin(kR) - kR\cos(kR)]$$

In this approach $\sigma(R)$ is taken around one when $R = 8h^{-1}Mpc$ because of measures performed observationally. Then, normalizing the power spectrum would imply to force $\sigma(R)$ to be one for the mentioned distance.

But several problems arise, one is that this normalization is not precisely valid for linear regime since $\sigma(R) \approx 1$ when $\delta(R) \ll 1$. Other one is baryonic matter is probably a bias tracer of the mass distribution.

It is necessary to consider that after recombination epoch, density perturbations started growing in size causing a non linear growth to appear. This implies a change in the density field and likewise the power spectrum.

2.8 Baryonic acoustic oscillations

Let us consider the epoch before recombination. The baryonic plasma (ionized protons and electrons) was coupled with radiation via Thomson scattering, i.e., the electric field of photons accelerate charged particles making small density perturbations to disperse. Nevertheless, considering that dark matter do not interact with radiation, small dark matter density contrasts can form. Hence, the baryons are subject to two competing forces, radiation pressure and gravitation. Consider a particular dark matter density contrast that attract nearby baryons, they start clustering around the dark matter forming a bigger density contrast. But, due to the pressure caused by coupling, the outward force becomes bigger than gravity, making baryons to move outward as a sound wave. This oscillation of the baryonic plasma is known as baryonic acoustic oscillation.

When decoupling occurs and temperature drops, the force responsible for the expansion of the shell disappear, this is, the pressure caused by the coupling between baryons and radiation, leading baryons in the last position they were located. The scale of the baryonic acoustic oscillation is usually called the sound horizon and it can be computed as

$$s = \int_{z_{rec}}^{\infty} \frac{c_s dz}{H(z)}$$

where c_s is the velocity of the propagation and $H(z)$ is the hubble param, ([**?**]).

Therefore, there is a spherical shell formed around the dark matter density perturbation. Now, not only dark matter density contrast seed gravitational instability but the baryons in the shell as well.

The structures continue to grow reaching non linear growth and wipe out the imprint lead by the baryonic acoustic oscillations except for the bigger ones. The estimated size of the remaining BAO is 150 Mpc, causing that scale to be more likely to have galaxy formation activity. The reason this distribution is not observed at cosmological scales is because of the amount of imprints, they smear out the preferred scale. Though, it is expected an enhancement in the two point correlation at scales of the baryonic oscillations. As was seen before, there is a direct correspondence between the two point correlation and the power spectrum. Hence, a characteristic oscillation in the power spectrum caused by the imprint of BAO is naturally found.

Since baryonic acoustic oscillations are primarily a linear phenomenon, they are preserved in the power spectrum despite of the temporal evolution. Then, BAO are used as an standard ruler, specifically for high redshift where other rulers tend to fail. This is commonly used for constraining dark matter models.

Although, the nonlinear collapse change the shape and position of baryonic acoustic oscillations, broaden and shift the peak. This is clearly seen in the figure (2.7), the broadening of the peak initially shown as a very sharp causes a damping in the frequency in the power spectrum. It is expected that this effect that is going to be studied in this work, affects baryonic acoustic oscillations on scales around $\sim 10 \text{Mpc}$.

The diffusion damping (silk damping) also causes a reduction in size of density inequalities by the diffusion of photons from hot regions to colder ones during the epoch of recombination.
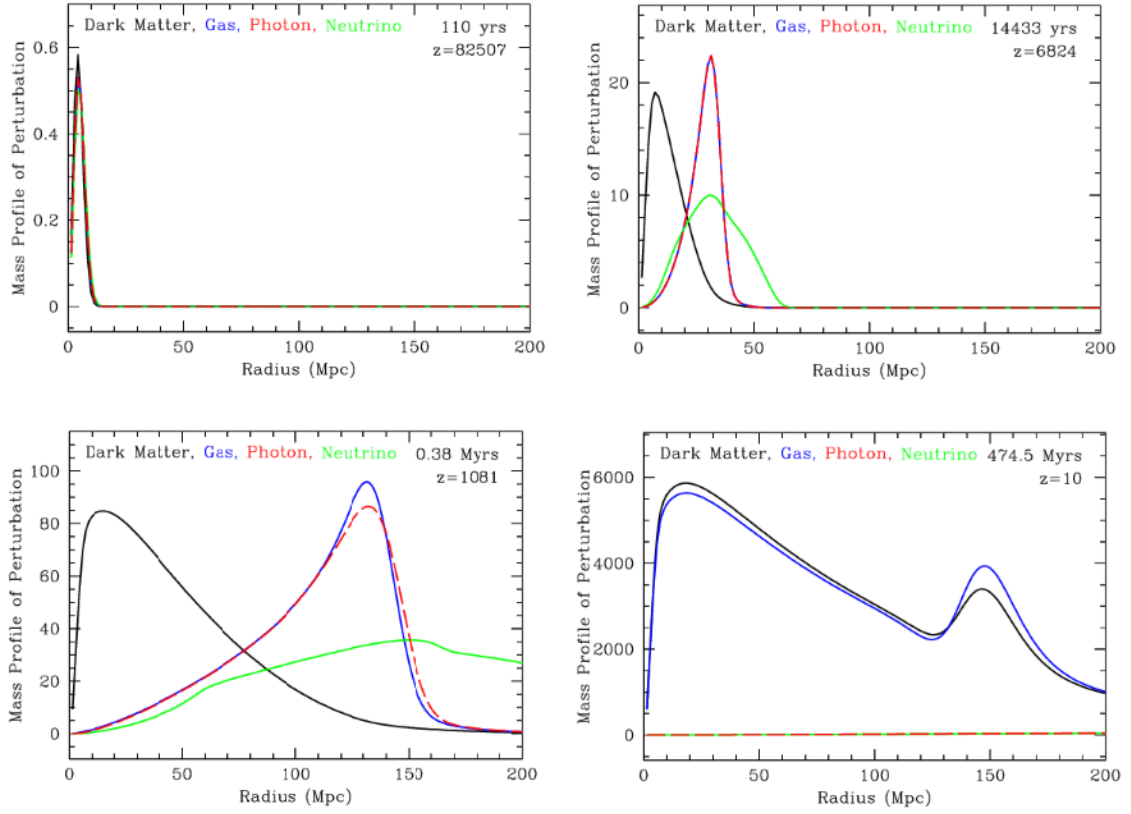
Figure 2.6: All the figures show the evolution of the radial mass profile of dark matter, baryons, photons and neutrinos. First one: Initial perturbations of the four species. Second one: the neutrinos do not interact and move away, the plasma of baryons and radiation overdensity expands because of radiation pressure, the dark matter continues to fall in the perturbation. Third one: The temperature drops enought to lead to decoupling, the baryons slows down until stopped, the radiation and neutrinos continue moving away. Fourth one: The dark matter and baryons eventually get the same distribution because of the gravitational interaction.
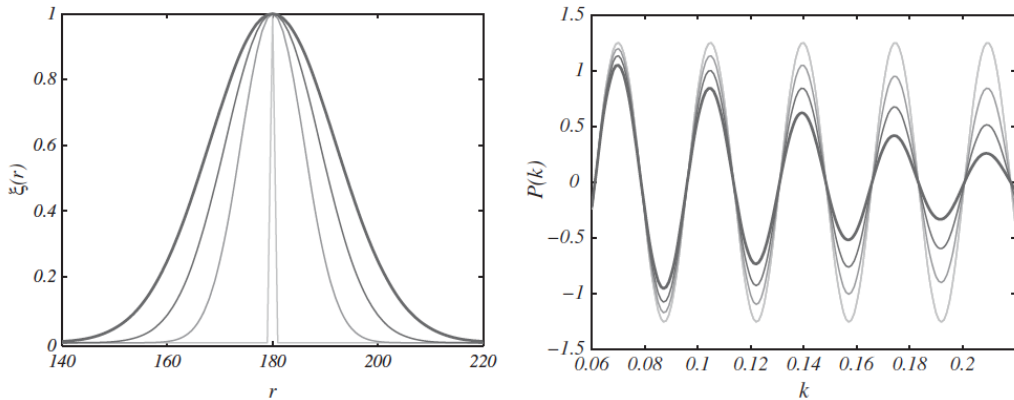

Figure 2.7: In the left the correlation function and the right the power spectrum. When the width of the peak is increased the acoustic oscillation obtained in the power spectrum is damped.

CHAPTER 3

Cosmological simulations

Currently in cosmology, one issue is to find the way the dynamics of the Universe evolves from its first stages to the actual epoch. Computational resources appear as a necessary tool to tackle such problems due to the big amount of interacting particles. If all possible components of the Universe would be considered in its evolution, the particles required to simulate the interaction among them would be so huge that it would not be viable to predict the evolution of every single particle. Hence, numerical approximations must be developed to find for every time step all the properties needed to describe the system, even when particles studied have masses with magnitude order of several stellar masses.

In cosmological simulations a key component to consider is dark matter, since it is mostly because of this one that the Universe has a filament structure. The latter asseveration is due to dark matter dominates the gravitational interaction, not only because of its amount compared to baryonic matter but also because it only interacts in this way.

This component cannot be observed directly cause it does not interact with radiation. But, since its gravitational effects are strong, there are observational evidence that accounts for its existence. For example, observing galaxy rotation curves, the velocity measured at the outskirts of spiral galaxies was too fast to explain with only baryonic matter.

Defining as total density the sum of baryonic and dark matter, a key argument to ignore baryonic matter in simulations can be given, dark matter would contribute with around 80% of all this density content. Hence, the assumption that the Universe dynamics is determined by dark matter is plausible.

The next chapter is divided in several sections, the first one corresponds to the methods used in cosmological simulations to calculate the gravitational evolution of the system. The second one contains different criteria selection to detect a dark matter halo in simulations. The third and fourth sections are dedicated to explain how to build two different statistical measures of clustering in real space, the correlation function and in fourier space, the power spectrum. The text books and articles that are used as reference in the next chapter are [5], [2], [6], [7], [8], [9], [10], [11].

3.1   Numerical methods

To study the Universe evolution at big scales, simulations of dark matter interacting particles inside a cosmological boxe are performed. In such cases is necessary to suppose initial conditions, an initial configuration of the Universe, i.e., an initial density field or an initial shape for the power spectrum. As mentioned, in these cosmological simulations dark matter is a key component, in many cases is the only particle considered. Hence, it is important to provide some observational evidences encountered. As already stated dark matter does not interact with radiation, nevertheless it turns out that the gravitational effects that causes are esential for the dynamical evolution of the Universe. It is around the $\sim 24\%$ content of the Universe.

One of the first observational evidence was found in the Coma cluster due to a mass estimation from the virial theorem, let us see this in more detail: the specific kinetic energy of the system is $T = v^2/2 \sim 3\sigma^2/2$ where σ is the galaxy velocity dispertion and the potential energy is $U = 3GM_{vir}/(5R_{vir})$. From the mass-luminosity ratio and the mean luminosity of the cluster, a second estimative of the mass is found. There is such a big discrepancy between the two values that is reasonable to affirm that $\sim 90\%$ of the cluster's mass is not visible.

The rotation curve of the galaxies can be other prove for dark matter existence, for example, the velocity measures performed with respect to the radious of Andromeda galaxy (or another spiral galaxies) is approximately the same independent of the radial distance of the stars to the center of the galaxy. From this, it could be affirmed that density is uniform along the galaxy contrary to expected for the observed number of star in function of the radius.

Another example is the Bullet cluster, composed by two two clusters that are colliding, an event not commonly observed. The gas of them reaches velocities around ~ 10 *millions of miles*$/h$ during the violent collision while they interact among them because of their

charge. This interaction disminishes the gas velocity but this does not happen with dark matter cause it does not interact electrically. Using gravitational lensing a distortion map is obtained. Using the X rays detected and the distortion map, four different groups of matter are found, 2 bigger ones that correspond to the dark matter component and two smaller ones that correspond to luminous matter formed from the intercluster gas. These presents a strong evidence of dark matter existence.

So, additional to the initial conditions, the box size L and the number of dark matter particles N^3 that would be used should be fixed. The gravitational interaction calculation of such a big number of particles could in principle be calculated through direct sum of forces. This first attempt is not very efficient or even it is not possible to perform since the computing time or the computational resources would be very big to be viable. The latter is the reason for approximate methods to appear as a possible solution that implies more reasonable computing times.

A main objective in a simulation could be the study the formation process, fusion and further interactions that are produced among halos and vacuum regions that conform the filamentary structure of the Universe. Next, three of the most known numerical methods for cosmological simulations are going to be briefly exposed.

1. **Particle Mesh (PM)**[6]

   In this method a grid is created over the particle array as shown in the figure 3.1. The particles more closed to a vertice are assigned to this, to an specific cell, getting the density. Other way to calculate the density is cloud in cell, later explained in more detail, where particles are considered constant density cubes causing that a single particle contributes to different cells. Using Poisson equation the potential in every grid vertice can be found thanks to the Fourier transform. The potential calculation or the force of each particle can be interpolated among the points created by the grid.

   Although this method reduces considerably the computing time since its of the order of $O(N + M \log M)$ with N being the number of particles and M the number of vertices. The lack of resolution in the regions that are more dense makes this method insufficient to respond for the physical situation. Furthermore, it does not give account for a complex geometry or systems higly correlated. A step forward in this direction is P^3M that uses for smaller scales finer calculations making a particle particle calculation.
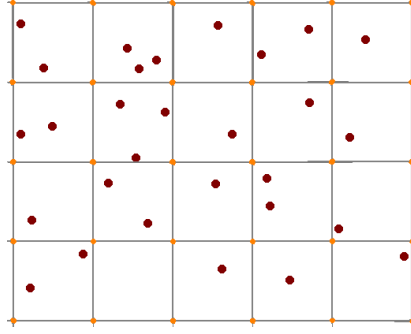
Figure 3.1: Particle mesh method. Every vertice of the grid gets properties calculated from the closer particles.

2. **Tree method**[6]

   To illustrate this method let us consider a 2D particle array. This square is divided in small cells of the same area where each particle is assigned to a specific cell. If this number is superior to one, subdivisions of the cell are performed and if the number of particles per subcells is superior to one, again subdivisions are made. This process is repeated until for every cell there is at most one particle. This subdivision is used to create a tree structure, this consists in a root, i.e., all the square area and the branches that are created with each subdivision performed. This serves as a map of the disposition of the particles in the square array. The particles are numerate from the upper left of the square until all particles in the first cell are numerate following with the second cell until the lower left is reached.

   When the gravitational calculation is performed, the contribution to the force exerted over a particle due to the more distant ones is much lower than with the nearer ones. Thus, the far ones can be approximated as a seudoparticle with mass M and with a position $r_{CM} = \sum_i m_i r_i / M$. As a selection criteria the next expression is taken

$$s/q \leq \theta \tag{3.1}$$

   where s is the cell size with wich the particle of interest is interacting with, d the distance cell particle and θ is a tolerance value to define. When the condition is satisfied the gravitational interaction is calculated directly with the seudoparticle. In the opposite case the relation 3.1 for the subcells that contain the studied cell and that way successively until the condition is satisfied or only one particle is present per cell. In this way the direct calculation is avoided for far objects without avoiding the calcu-

lation for the nearer ones. Therefore, the computing time is reduced from $O(N^2)$ to $O(N\log(N))$.
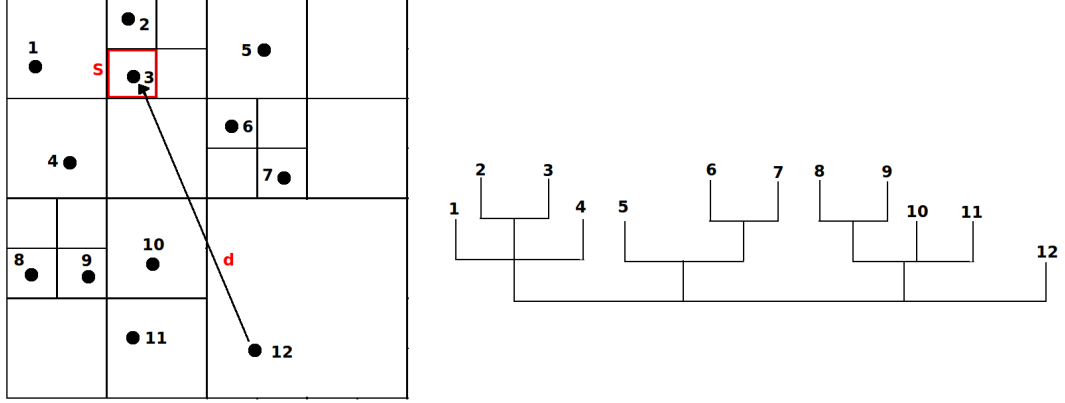

Figure 3.2: In the left panel is shown the array of the particles and the subdivisions performed until at most one particle is found per cell. In the right one, the tree found for such distribution is shown.

3. **ART Code[7]**

As its acronym indicates, Adaptive Refinement Tree Code consists in a multigrid code. An initial grid is created where the Poisson equation is solved followed by a refinement according to overdensities that are in certain regions. Even after performing the refinement over the grid, this calculation can be done continously. Here, calculations particle particle are not being performed. Something new compared to the methods previously exposed is that the cell shape can take any form allowing to get an adaptive grid depending on the amount of particles in the region.

There are many methods that are hibrid among the 3 exposed, for example the already mentioned P^3M. All of them have both advantages and disadvantages that need to be evaluated according to the needs of the simulation.

3.2   Halo selection

As a result of the dark matter particle interactions, perturbations grow enough to form ligated objects thus they are in virial equilibrium, these are known as dark matter halos and satisfy the relation $E_k = -V/2$. They are responsible for the potential wells that causes baryonic

matter to fall in, forming finally the galaxies we observe today, i.e., dark matter halos host galaxies.

A main result of a cosmological simulation are the dark matter halos catalogue, which we are going to work with, that contains halo properties such position, velocity, mass, radius and redshift. Therefore, a key step is to identify halos from a cosmological simulation, the methods generally use to acomplish such task are FOF and BDM[1]

1. **Friend of Friends (FOF)**

   To identify if a particles group lies in a dark matter halo, i.e., particles are linked, a length is defined such that all the particles that lie inside are part of the same group. This distance is called linking length. A condition is imposed, groups can not intersect among them, hence a particle can only belong to a specific group. But there is a problem with this approach, even when there is a little amount of particles in common between two groups, some sort of small "bridge" that unites both of them, they are selected as one group not two as would be expected. This method also allows to define substructures, therefore using different linking lengths, groups inside groups would be obtained, the bigger ones would host the smaller ones.

2. **Bound Density Maximun(BDM)**

   For this method the local maximum densities in the particle array of the simulation are detected. From them, a spherical cut is defined and the particles inside form the dark matter halo. Particles with bigger or equal velocity than the scape one are not included in the halo. Contrary to FOF method, halos can overlap while the center of mass of one halo does not fall into the other one. Nevertheless, if the center of mass of one halo falls in the virial radius of other one, the first one is considered a subhalo of the last one. The standard overdensity limit of the halos is $360\rho_{back}$ where ρ_{back} is the background density.

3.3   Density field in a cosmological simulation

To construct a good approximation of the real density field from a cosmological simulation, a sampling of the continuous density field in a regular grid of size N^3 is performed, the subdivisions created are called cells. Hence, an assignment of the particle charge, i.e. particle mass, to the grid must be done. To obtain a more realistic density field approximation the

---

[1] https://www.cosmosim.org/cms/simulations/halo-finders/

grid points can be increased also disminishing problems due to numerical effects but it is more expensive computationally. Furthermore, the number of particles in a simulation is a restriction to the maximum value that N can have, it can not exceed $\sqrt[3]{N_p}$, there would not be enough particles to map correctly the density field per cell. A size grid around the value mentioned would optimal in the sense that the particle mean per cell would be one, hence a Poisson distribution would be followed. But the sampling made from the particle distribution is not a mere sampling but a sampling convolved with a window function (the way a particle mass is distributed in the grid), i.e., the window function W that is used affects the density field calculated.

Since the particles are located in a specific position it can be assured that the particle number density is

$$n_0(\mathbf{x}) = \sum_{i=1}^{N_p} \delta^D(\mathbf{x} - \mathbf{x}_i)$$

where $\mathbf{x}_i$ the position of the i-th particle. The window function quantifies how much of the particle number density is distributed to a grid point separated by $\mathbf{x}$, hence the sample particle number density can expressed as

$$n(\mathbf{x}_p) = \int_V d^3x' n_0(\mathbf{x'})W(\mathbf{x}_p - \mathbf{x'})$$

Similarly, the sampled density contrast defined as $\delta^s(\mathbf{x}) = n(\mathbf{x}_p)/\bar{n} - 1$ can be found using the convolution of the real density contrast and the window function

$$\delta^s(\mathbf{x}) = [\delta * W](\mathbf{x}) \tag{3.2}$$

its fourier transformation is simply the product of the fourier transformation of the real density contrast and the window function

$$\delta^s(\mathbf{k}) = \delta(\mathbf{k})W(\mathbf{k}) \tag{3.3}$$

thus, the real density contrast can be obtained dividing the sampled density contrast with the window function used.

The procedure of convolving with a window function can be seen in a different way, if a point spreading or cloud shape function $S(x')$, being x' the distance from the particle position x_i, is carried by each particle then the charge assigned to the grid point x_p is given by the overlap of the shape function within the cubic cell p

$$W(x) = \int \Pi\left(\frac{x'}{H}\right) S(x' - x) dx'$$

where $\Pi(x)$ is the top hot function and $H = L/N$ is the size of a cell.

There are 3 commonly used schemes for the mass assignment, nearest grid point, cloud in cell and triangular shaped cloud. For each case we are going to consider a one dimensional window function. The sencond and third one are first and second order distribution schemes respectively, hence each of them is a better approximation than the previous one.

1. **Nearest grid point:** The first scheme considers that the particle charge is assigned to the cell where the particle falls, each cell is centered in a grid point, therefore the particle is assigned to the nearest grid point. Let us see this in more detail. If the cloud shape interpretation is used, the particle shape would be a Dirac delta function that would be assigned to the specific cell where particle falls in as shown in the figure 3.3 (a). If the other interpretation is considered, the window function would be a top hat function centered in the particle, the value assigned to grid point would the one that top hat function would get when is evaluated in that grid point as shown in figure 3.3 (b).

$$\begin{aligned} W_{NGP}(x) = \Pi\left(\frac{x}{H}\right) &\equiv \frac{1}{H}\Pi\left(\frac{x}{H}\right) * \delta\left(\frac{x}{H}\right) \\ &= \frac{1}{H}\Pi\left(\frac{x}{H}\right) * S\left(\frac{x}{H}\right) \end{aligned}$$

This window function in the fourier space is

$$W_{NGP}(k) = sinc\left(\frac{\pi k}{2k_N}\right)$$

where k_N is the Nyquist frequency that later will be defined.

2. **Cloud in cell:** This scheme assumes that the charge of a specific particle assigned to a grid point is given by the overlap of a cell with a size H centered in the particle with the cell centered any the grid point. Then, the particle not only contributes to the cell where it falls in but also to some of the 26 neighbour cells. This explanation is shown in the left figure of 3.4 but according to the window function explanation, a "triangle" function $\Lambda(x)$ centered in the particle and length H is evaluated in the corresponding
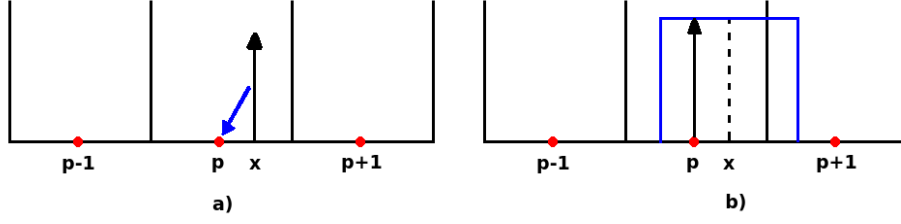
Figure 3.3: The left figure shows the cloud shape interpretation where the Dirac function is assigned to the particle grid. The right one shows the window function interpretation where the top hat function evaluated in the grid point would give the charge assigned to it.

grid points of the cells, the one where particle falls in and the neighbour ones, finding the contribution of the charge to every one of them as shown in figure 3.4 (b).

$$
\begin{aligned}
W_{CIC}(x) = \Lambda\left(\frac{x}{H}\right) &\equiv \frac{1}{H}\Pi\left(\frac{x}{H}\right) * \Pi\left(\frac{x}{H}\right) \\
&= \frac{1}{H}\Pi\left(\frac{x}{H}\right) * S\left(\frac{x}{H}\right)
\end{aligned}
$$

This window function in the Fourier space is

$$
W_{CIC}(k) = sinc^2\left(\frac{\pi k}{2k_N}\right)
$$

hence, the Fourier transform of the CIC window function is the square of the Fourier transform of the NGP window function.
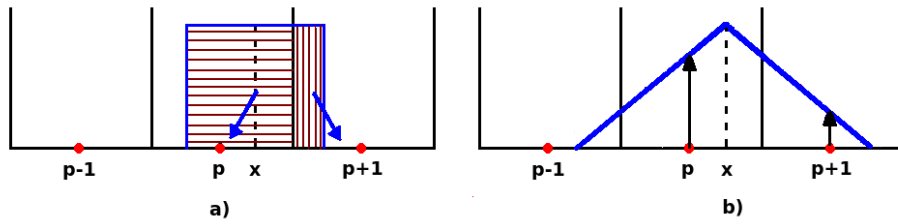

Figure 3.4: The left panel shows the CIC cloud shape function and the intersection between the cell centered in the particle with the cells provides the contribution of the charge to every cell. The right one shows a "triangle" function that is evaluated in every grid point to find the charge contribution to the cell.

3. **Triangular shaped cloud:** This scheme is as the two previously presented but the cloud shape and window function change. As it happens with CIC, TSC contributes to different cells, not only the one where it falls in. Both interpretations are shown in the

figure 3.5. Next the expression to calculate the charge contribution to a specific cell is given by

$$
\begin{aligned}
W_{TSC}(x) &= \frac{1}{H}\Lambda\left(\frac{x}{H}\right) * \Pi\left(\frac{x}{H}\right) \\
&= \frac{1}{H}\Pi\left(\frac{x}{H}\right) * S\left(\frac{x}{H}\right)
\end{aligned}
$$

The Fourier transform of the window function is

$$
W_{TSC}(k) = sinc^3\left(\frac{\pi k}{2k_N}\right)
$$

hence, the Fourier transform of the TSC window function is the cubic of the Fourier transform of the NGP window function.
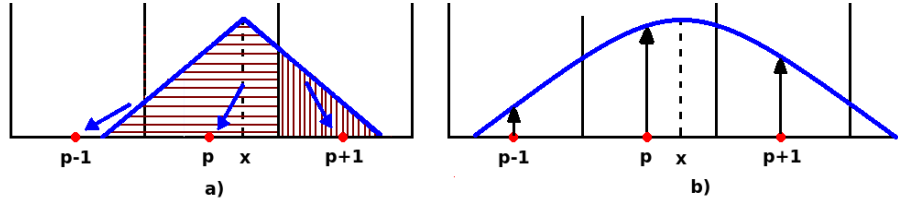

Figure 3.5: The left figure shows the cloud shape function, a "triangle" function and the overlap with the cells provides the value of the charge assigned to every cell. But using the window function interpretation the right figure is obtained, where the particle carries with a function that evaluated in every grid point gives the contribution to the specific cell.

Hence, each successively higher order assignment function is obtained by convolving the previous assignment function with $\frac{1}{H}\Pi\left(\frac{x}{H}\right)$.

From a one dimensional window function can be obtained the three dimensional one, simply as the multiplication of the three one dimensional ones. This last asseveration is valid due to the grid used is regular.

Thus, for every cell contained in the cosmological box a value of the convolved density field is calculated using a specific mass assignment scheme.

3.4   Power spectrum in cosmological simulations

The density perturbations of the ensemble, convolved density field for every cell of the box, allow to calculate the power spectrum as shown in equation 2.14, an esemble average for every

mode κ. Since this a statistical measure in the Fourier space let us see the Fourier transform in more detail.

3.4.1   Fourier transform

The fourier transform is defined for this work with the next convention

$$F(\boldsymbol{\kappa}) = \int_{-\infty}^{\infty} d^3x f(\mathbf{x}) e^{-i\boldsymbol{\kappa}\cdot\boldsymbol{x}} \tag{3.4}$$

with κ being the wave number vector. The inverse fourier transform as

$$f(\boldsymbol{x}) = \int_{-\infty}^{\infty} \frac{d^3\kappa}{(2\pi)^3} F(\boldsymbol{\kappa}) e^{i\boldsymbol{\kappa}\cdot\mathbf{x}} \tag{3.5}$$

The convolution of the functions $g(\mathbf{x})$ and $f(\mathbf{x})$ is defined as follows

$$h(\mathbf{x}) = |\mathbf{g} * \mathbf{f}|(\mathbf{x}) \equiv \int_{-\infty}^{\infty} \mathbf{g}(\mathbf{x}')\mathbf{f}(\mathbf{x} - \mathbf{x}')\mathbf{d^3 x'}$$

but the Fourier transform of $h(\mathbf{x})$ is

$$H(\boldsymbol{\kappa}) = G(\boldsymbol{\kappa})F(\boldsymbol{\kappa})$$

this is known as the convolution theorem. It is used in our work since the fourier transform of the window function convolved with the density field (equation 3.2) allow us to obtain the real density field. From equation 3.3

$$\delta(\mathbf{k}) = \delta^s(\mathbf{k})/W(\mathbf{k})$$

In the situation we are dealing with, the function $F(\boldsymbol{\kappa})$ is only sampled at evenly spaced intervals (N^3 frequencies totally) since we only know $f(\mathbf{x})$ in N^3 points

$$F(\boldsymbol{\kappa}) = \begin{cases} F(\kappa_F \boldsymbol{n}_\kappa) & \boldsymbol{n}_\kappa = (i, j, k) \in Z^3 \\ 0 & \text{otherwise} \end{cases}$$

where $\kappa_F = 2\pi/L$ is the fundamental frequency.

Due to the functions are only sampled in specific points, the integrals defined in equations 3.4 and 3.5 can be approximated to the discrete Fourier transform. Let us express them in terms of the density fluctuations in real and Fourier space because they are the ones of interest for our work

$$\delta(\boldsymbol{\kappa}_p) = H^3 \sum_{n_p} \delta(\boldsymbol{r}_p) e^{-i\boldsymbol{\kappa}_p \cdot \boldsymbol{x}_p}$$

$$\delta(\boldsymbol{r}_p) = \frac{1}{L^3} \sum_{\boldsymbol{k}_p} \delta(\boldsymbol{\kappa}_p) e^{i\boldsymbol{\kappa}_p \cdot \boldsymbol{x}_p}$$

where $H = L/N$ is the separation of the grid in the real space, $\boldsymbol{\kappa}_p = k_F \mathbf{n}_p$ and $\boldsymbol{n}_p = (i, j, k)$ with each index varying from $-N/2 \leq i, j, k \leq N/2$. The function $\delta(\boldsymbol{r}_p)$ is sampled in the points $\boldsymbol{r}_p$ and $\delta(\boldsymbol{\kappa}_p)$ in the points $\boldsymbol{\kappa}_p$. Therefore, the Fourier space is divided into small cells, N cubes of size $\kappa_g = 2\pi/H$ per dimension as it was done for the simulation.

Furthermore, the extreme values for $\boldsymbol{n}_p$ correspond to Nyquist critical frequency

$$\kappa_N = \pi \frac{N}{L} = \frac{\pi}{H}$$

so $-\kappa_N < k < \kappa_N$. A phenomenon called aliasing appears when a continuous function is sampled and is not bandwidth limited to a frequency smaller than κ_N. It consists in a folding over or aliasing of the frequencies that fall outside the range as shown in figure 3.6.
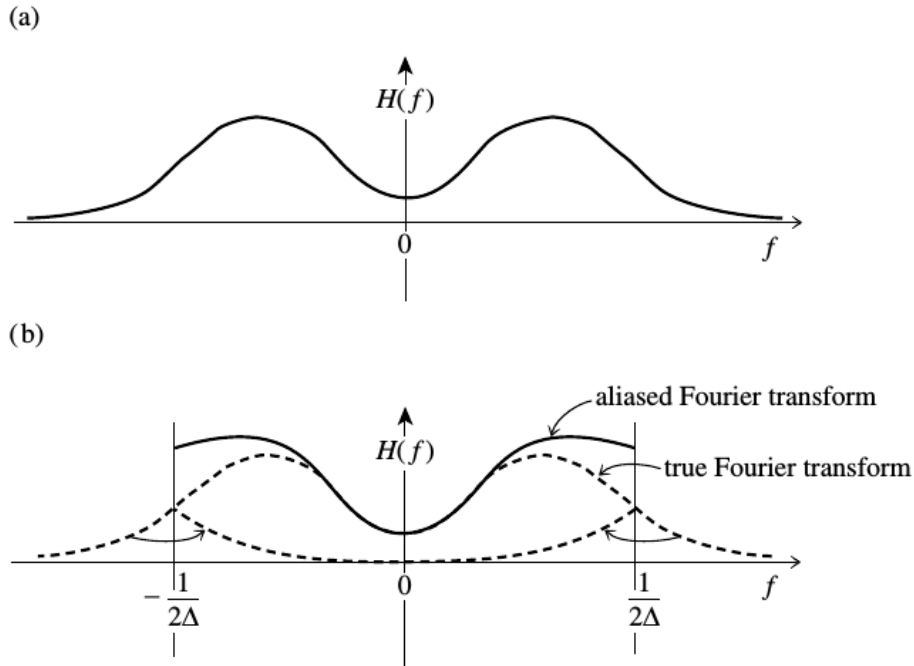

Figure 3.6: Aliasing effect for $H(f)$ sampled with a space interval Δ. Frequencies outside the frequency range are included into the range because of the discrete sampling of the function. Figure taken from [12].

To perform the discrete Fourier transform of the sampled density field was used the free library FFTW, where a fast Fourier discrete transformation (FFT) is implemented. Because of algorithmic details of the FFT the fourier coefficients are ordered in the following manner

$$\kappa_l(i) = \begin{cases} \frac{2\pi}{L}i & \text{if} \quad i = 0, \ldots, \frac{N}{2} \\ \frac{2\pi}{L}(-N+i) & \text{if} \quad i = \frac{N}{2}+1, \ldots, N-1 \end{cases}$$

where the subindex l stands for x, y or z coordinate. The library has different routines, one is a complex to complex function, this is, perfoms a Fourier transformation of a sampled complex function. Other one, named real to complex routine, takes the real samples of a function to find the Fourier transformation. The last one uses the Hermitian condition that allows to improve the calculation in speed and memory usage

$$\delta_\kappa(-\mathbf{n}_\kappa) = \delta_\kappa^*(\mathbf{n}_\kappa)$$

where the superscript $*$ denotes complex conjugate. In both cases a normalization must be taken into consideration, this can be noticed in the relation between the transformed density field obtained with FFTW and the sampled space density field

$$\delta^{FFTW}(\mathbf{n}_k) = \sum_{r_p} \delta(\mathbf{r}_p)e^{-i\boldsymbol{\kappa}_p \cdot \boldsymbol{r}_p} = \frac{\delta(\boldsymbol{\kappa}_p)}{H^3}$$

with the last expression and the definition of PS given in equation 2.14, the power spectrum from FFTW is given by [5]

$$P(\kappa_F n_1) = \frac{H^6 k_F^3}{(2\pi)^3}\langle \delta^{FFTW}(\boldsymbol{n}_1 \delta^{FFTW}(-\boldsymbol{n}_1)\rangle = \frac{V}{N^6}\langle|\delta^{FFTW}(\boldsymbol{n}_1)|^2\rangle \tag{3.6}$$

this is the power spectrum estimator that is used throughout this work.

3.4.2 PS calculation

To calculate the power spectrum, the next steps are followed

1) From a cosmological box of size L, a grid with N^3 subdivisions is performed creating cells of volume H^3.

2) The sampled space density field is created using a specific window function, mass of particles are assigned to the grid.

3) With FFTW software, the FT of the sampled space density field is calculated.

4) To deconvolve and eliminate the aliasing effect $P(\boldsymbol{\kappa}) \equiv |\delta(\kappa)|^2$ is divided by the next window function, at each grid point or equivalently each cell

$$W(\boldsymbol{\kappa}) = \prod_{i=1}^{3} \left[1 - \frac{2}{3} \sin^2 \left(\frac{\pi \kappa_i}{2 \kappa_N} \right) \right]$$

where $\boldsymbol{\kappa} = (\kappa_x, \kappa_y, \kappa_z)$ as proposed in [13].

5) The amount $P(\kappa)$ is calculated taking the spherical average of $P(\boldsymbol{\kappa})$ corrected inside the shell $\kappa - \Delta\kappa/2 < |\boldsymbol{\kappa}| < \kappa + \Delta\kappa/2$.

3.5   Correlation functions in cosmological simulations

In practice, to calculate in a cosmological simulation the correlation function a at distance r, it has to be performed an average of the number of neighbours per particle at a given scale or the binned comoving separation. In this direction correlation function estimators can be used, one of the most basic ones is shown below. Two catalogues are considered for this estimator, one is the properties of the particles of the box, data-data catalogue (DD) and the second one is generated randomly with at least the same number of particles and the same size of the box, random-random catalogue (RR). The DD catalogue should have regions with more or less clustering than a homogeneous distribution, this is precisely the RR catalogue role, a way to measure how much the DD catalogue deviates from the homogenous distribution.

From this estimator is easier to notice that $\xi(r)$ is a measure of excess or deficiency of clustering at r making it more intuitive

$$1 + \xi(r) = \frac{\eta_{DD}(r)}{\eta_{RR}(r)}$$

here $\eta_{RR}(r)$ is the number of pairs of particles at a distance r in the catalogue DD and $\eta_{RR}(r)$ is the number of pairs of particles at a distance r in the catalogue RR.

Other common estimators also need an additional catalogue, the data-random, where the pair of particles would not only include the DD or RR but a mixed catalogue containing both arrays, making more robust the estimator proposed [14]

$$\text{Landy-Szalay Estimator} \quad \xi_{LS}(r) \;=\; 1 + \frac{DD(r)}{RR(r)} \left(\frac{N_R}{N} \right)^2 - 2 \frac{DR(r)}{RR(r)} \left(\frac{N_R}{N} \right)$$

$$\text{Hamilton Estimator} \quad \xi_{HAM}(r) \;=\; \frac{DD(r)RR(r)}{DR(r)^2} - 1$$

where N_R is the number of points of the RR catalogue and N of the DD catalogue.

3.5.1   Correlation function calculation

To calculate the correlation function the Landy-Szalay estimator is used, the next rough steps are followed to calculate it

1) A catalogue of N_R particles is generated randomly in a cubic box of size L.

2) For a bin around r the magnitude of the distances between DD, RR and DR particles are found, that way, pairs of galaxies that are at a distance r for every catalogue are obtained. Finally, using Landy-Szalay estimator the correlation function is calculated for each radial bin.

References

[1] P. "Ade, N. Aghanim, and e. a. Akrami, "Planck 2015 results. XVI. Isotropy and statistics of the CMB," *Astron. Astrophys.*, vol. 594, p. A16. 62 p, Jun 2015.

[2] M. S. Longair, *Galaxy Formation.* Springer, second ed.

[3] H. Mo, F. van den Bosch, and S. White, *Galaxy Formation and Evolution.* Cambridge University Press, 2010.

[4] T. Padmanabhan, *Cosmology and Astrophysics Through Problems.* Cambridge University Press, 1996.

[5] D. Jeong, *Cosmology with high (z > 1) redshift galaxy surveys.* Doctoral dissertation, The University of Texas, 2010.

[6] S. Pfalzner and P. Gibbon, *Many-Body Tree Methods in Physics.* Cambridge University Press, 1996.

[7] A. Klypin, "Numerical simulations in cosmology i: Methods," 2000.

[8] A. Klypin, "Numerical simulations in cosmology ii: Spatial and velocity biases," 2000.

[9] A. Klypin, "Numerical simulations in cosmology iii: Dark matter halos," 2000.

[10] Y. P. Jing, "Correcting for the alias effect when measuring the power spectrum using a fast fourier transform," *The Astrophysical Journal*, vol. 620, no. 2, p. 559, 2005.

[11] F. Montesano, A. G. Sanchez, and S. Phleps, "A new model for the full shape of the large-scale power spectrum," *Monthly Notices of the Royal Astronomical Society*, vol. 408, no. 4, pp. 2397–2412, 2010.

[12] W. H. Press, S. A. Teukolsky, W. T. Vetterling, and B. P. Flannery, *Numerical Recipes 3rd Edition: The Art of Scientific Computing*. New York, NY, USA: Cambridge University Press, 3 ed., 2007.

[13] D. Jeong and E. Komatsu, "Perturbation theory reloaded. ii. nonlinear bias, baryon acoustic oscillations, and millennium simulation in real space," 2009.

[14] M. J. P. Borderia, V. J. Martinez, D. Stoyan, H. Stoyan, and E. Saar, "Comparing estimators of the galaxy correlation function," *The Astrophysical Journal*, 1999.